Drug Design, Development and Therapy

Dovepress
open access to scientific and medical research

Open Access Full Text Article

ORIGINAL RESEARCH

Therapeutic Effects of Hydrogel Formulations Incorporating Troxipide Nanoparticles on Oral Mucositis in Hamsters

Reita Kadowaki[1], Fumihiko Ogata[1], Miku Nishida[1], Miri Komatsu[1], Hiroko Otake[1], Yosuke Nakazawa[2], Naoki Yamamoto[3], Naohito Kawasaki[1], Noriaki Nagai[1]

[1]Faculty of Pharmacy, Kindai University, Higashi-Osaka, Osaka, Japan; [2]Faculty of Pharmacy, Keio University, Minato-ku, Tokyo, Japan; [3]Support Office for Bioresource Research, Research Promotion Headquarters, Fujita Health University, Toyoake, Aichi, Japan

Correspondence: Noriaki Nagai, Faculty of Pharmacy, Kindai University, 3-4-1 Kowakae, Higashi-Osaka, Osaka, 577-8502, Japan, Tel +81 6 4307 3638, Fax +81 6 6730 1394, Email nagai_n@phar.kindai.ac.jp

Purpose: Medical therapies, such as the use of anti-inflammatory agents, are commonly used for the treatment of oral mucositis (OM). However, these treatments have limited efficacy in treating severe cases of OM. In this study, we aimed to develop a carbopol gel incorporating troxipide (TRO) nanoparticles and methylcellulose (TRO-NP gel) and demonstrate its efficacy in accelerating wound healing in a hamster model of OM (OM model) induced by acetic acid injection.

Methods: TRO nanoparticles were prepared using bead milling. The crystalline form was determined by powder X-ray diffraction, and the particle size was measured using a NanoSight LM10 instrument. The drug release was determined using a Franz diffusion cell, and the hamsters injected with acetic acid were selected to evaluate the therapeutic effect of OM.

Results: After preparing TRO nanoparticles, we observed a mixture of crystals and amorphous TRO, and the particle size of TRO in the TRO-NP gel ranged from 50 to 280 nm. The TRO-NP gel exhibited a more uniform TRO distribution and viscosity compared to the Carbopol gel containing TRO microparticles (TRO-MP gel). However, the solubility of TRO was comparable in both TRO-MP and TRO-NP gels. The TRO-NP gel released a higher amount of TRO than that from the TRO-MP gel, with detectable release of TRO nanoparticles. TRO levels in the cheek pouches of hamsters treated with TRO-NP gel were higher than those treated with TRO-MP gel. The increased TRO levels in the cheek pouches of hamsters treated with TRO-NP gel were attenuated by treatment with 40 μM dynasore, an inhibitor of clathrin-dependent endocytosis (CME). Moreover, the therapeutic effect of the TRO-NP gel was superior to that of the TRO-MP gel in the hamster model of OM.

Conclusion: We have designed a TRO-NP gel, and this gel showed excellent TRO delivery into the cheek pouch tissue through the CME pathway. Moreover, the TRO-NP gel treatment enhanced wound healing after acetic acid injection.

Keywords: troxipide, nanoparticle, oral mucositis, hydrogel, endocytosis

Introduction

Oral mucositis (OM) results from direct cell injury caused by radiotherapy or chemotherapy, notably impacting patients' quality of life. Treatment approaches such as oral cryotherapy, brushing, topical granulocyte-macrophage colony-stimulating factor, disinfectant mouthwash, steroidal anti-inflammatory drugs, and mucosal coating agents are commonly employed.[1,2] A pilot randomized controlled trial evidenced that rebamipide mouthwash attenuated severe OM induced by chemoradiotherapy or radiotherapy.[3] However, since the efficacy of these treatments remains limited,[3,4] the development of alternative medical therapies for OM is necessary.

Troxipide (TRO), also known as 3,4,5-trimethoxy-N-3-piperidinyl, inhibits oxidative stress and neutrophil-mediated inflammation,[5–9] along with enhancing cytoprotective prostaglandins secretion.[10] Due to these properties, TRO is used to treat gastroesophageal reflux disease, and its mechanism may enhance the treatment of severe OM. However, TRO is primarily absorbed in the stomach,[11] and its uptake is hindered in OM due to the alkaline nature of this molecule

Received: 3 August 2023
Accepted: 7 November 2023
Published: 15 November 2023

Graphical Abstract

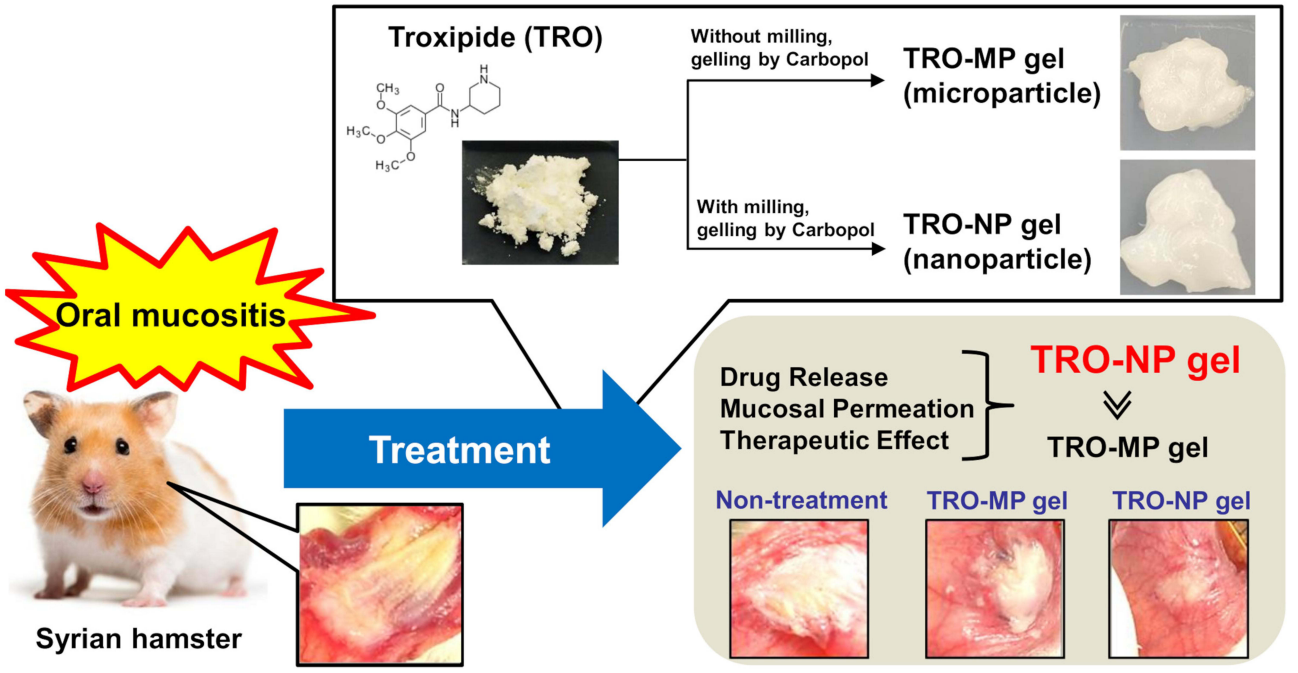

(pKa=10.08, pKb=3.92). Therefore, new technology is required to improve the absorption of TRO when locally applied to OM sites.

Nanotechnology has been increasingly used for transdermal and dermal drug delivery, and nanocrystals, liposomes, polymeric micelles, dendrimers, quantum dots, biodegradable nanoparticles, lipid nanocarriers, silica nanoparticles, nanoemulsions, and polymer-drug conjugates have been explored as drug delivery systems.[12–15] Nanoparticles have a large surface area compared to their small volume, with surface atoms dominating their physics and chemistry.[16–21] Their high surface energy enables the adsorption, binding, or transportation of other compounds, such as drugs, chemicals, or proteins, often exhibiting unusual catalytic properties.[22,23] In contrast, the transportation of particles >500 nm is almost completely blocked by excess sputum released under the condition of cystic fibrosis and gastrointestinal mucus.[24–26] Additionally, the increased surface area of nanoparticles enhances mucoadhesion.[27] Therefore, a formulation containing nanoparticles with an average particle diameter of <100 nm would be an appropriate carrier for TRO to treat OM effectively. Furthermore, it is crucial to select a suitable carrier base for TRO to facilitate local application. Gels are commonly employed as carriers for numerous drugs due to their local effects, lubrication properties, and percutaneous absorption. Carbopol® 934, also known as Carbopol or carboxypolymethylene, is a water-soluble hydrogel that facilitates drug release from transdermal formulations containing nanoparticles.[28–30] Thus, here, we aimed to develop a new Carbopol gel containing TRO nanoparticles (diameter: <100 nm) for direct application to the oral mucosa. Moreover, we investigated the wound-healing and preventive effects of this gel in hamsters injected with acetic acid (OM model) and validated its clinical relevance as an experimental system.

Materials and Methods

Animals

Sixty-eight male 7-week-old golden hamsters (Mesocricetus auratus) (Shimizu Laboratory Supplies Co., Ltd. Kyoto, Japan) were divided into two groups: one group (n=5×9=45) to determine changes in TRO content following gel treatment and another group (n=8+5×3=23) for assessing changes in wound area in the hamster OM model. The hamsters

were housed at 25 °C and provided with water and a standard CE-2 diet (Clea Japan Inc., Tokyo, Japan). The mean weight of the hamsters was 101±0.9 g. All animal experiments were conducted in compliance with the guideline of Kindai University, the Japanese Pharmacological Society, the Guide for the Care and Use of Laboratory Animals provided by the National Institutes of Health, the Animal Research: Reporting of In Vivo Experiments (ARRIVE) guidelines and the American Veterinary Medical Association (AVMA) euthanasia guidelines from 2020. The Animal Experimental Committee of the Kindai University approved the experimental protocol on April 1, 2019 (approval number: KAPS-31-016). Euthanasia was performed by injecting pentobarbital (200 mg/kg, i.p.) according to the AVMA guidelines 2020.[31]

Chemicals

Cytochalasin D, methyl p-hydroxybenzoate, 10% ammonia solution, and TRO (purity >98.0%) were purchased from Wako Pure Chemical Industries Ltd. (Osaka, Japan), while methylcellulose (MC) was obtained from Shin-Etsu Chemical Co. Ltd. (Tokyo, Japan). Additionally, we utilized Carbopol® 934 (Serva, Heidelberg, Germany), a Bio-Rad Protein Assay Kit (Bio-Rad, Hercules, CA, USA), pentobarbital (Tokyo Chemical Industry Co. Ltd., Tokyo, Japan), rottlerin and dynasore (Nacalai Tesque, Kyoto, Japan), and nystatin (Sigma-Aldrich, St. Louis, MO, USA). All chemicals used were of the highest grade of purity.

Gel Formulations Containing TRO Micro- and Nanoparticles

Gel formulations containing TRO nanoparticles (TRO-NPs) were prepared as described in previous reports.[28–30] TRO powder and MC were mixed using an agate mortar for approximately 30 min. The mixture was suspended in purified water to prepare a 2% TRO suspension (TRO-sus). The suspension was placed in a 2.0-mL tube containing 2.0 g zirconia beads (0.1 mm in diameter) and crushed at 1500 rpm for 3 h at 4 °C (milled TRO) using a Shake Master NEO (Bio-Medical Science Co. Ltd., Tokyo, Japan). Subsequently, TRO-sus and milled TRO were gelled by adding 3% Carbopol® 934, and gels containing micro- (TRO-MP) and nanoparticles loaded with 1.5% TRO were prepared, respectively. The pH of the gels was adjusted to 7.5 by 5% ammonia solution. The composition of the TRO-MP and TRO-NP gels was as follows: 1.5% TRO, 0.5% MC, and 3% Carbopol in distilled water (w/w%). Our previous study showed that 3% Carbopol® 934 was suitable to use as the gel base for the drug nanoparticles, since the gel showed a high release of drug nanoparticles, and it provided appropriate viscosity.[28] We determined the concentration of Carbopol® 934 by following methods from previous reports.

High-Performance Liquid Chromatography

The concentration of TRO was determined using a high-performance liquid chromatography (HPLC) LC-20AT system (Shimadzu Corp. Kyoto, Japan). The mobile phase comprised a 50 mM phosphate buffer/acetonitrile (90/10, v/v) at a flow rate of 0.25 mL/min. Samples from the gels were prepared by diluting in methanol. Moreover, the samples coming from biological samples (cheek pouches) were homogenized in methanol and were then centrifuged at 20.4×10^3 g and at 4 °C for 20 min. The blood was also centrifuged at 20.4×10^3 g and at 4 °C for 20 min. These supernatants were used to measure the TRO content in both the cheek pouches and blood samples. One hundred microliters of each sample were added to a sample cup. Subsequently, 50 µL methyl p-hydroxybenzoate (internal standard) in methanol was added. Thereafter, 10 µL sample was injected using a SIL-20AC auto-injector, and TRO was separated at 35 °C using an Inertsil® ODS-3 column in a CTO-20AC chromatography chamber (GL Science Co., Inc., Tokyo, Japan) and determined at 254 nm. The TRO peak eluted between 5 and 6 min, whereas that of the internal standard eluted at 14.5 min; the detection sensitivity was 25 ng/mL.

Particle Size

The dispersions and gels containing TRO nanoparticles were diluted 1000-fold with purified water, and the particle size and number of TRO nanoparticles were measured using a NanoSight LM10 (Quantum Design Japan, Tokyo, Japan). The time, viscosity, and wavelength for measurement were set at 60s, 1.45 mPas, and 405 nm, respectively. Atomic force microscopy (AFM) images of TRO in dispersions and gels containing TRO nanoparticles were obtained using a scanning

probe microscope SPM-9700 (Shimadzu Corp., Kyoto, Japan). The AFM images were obtained by combining the height and phase images of TRO.

Evaluation of the Crystalline Form

Changes in the crystalline form were determined using powder X-ray diffraction (XRD) and differential thermal analysis (DTA). The dispersions were lyophilized and used as samples for the XRD and DTA analyses. The freeze-drying was performed by using the FREEZE DRYER FD-1000 (TOKYO RIKAKIKAI CO., LTD., Tokyo, Japan), and the conditions of the lyophilization (freeze-drying) were as follows: temperature −20°C, pressure 20 Pa, and time 48 h. A Mini Flex II system (Rigaku Co., Tokyo, Japan) was used for XRD measurements. Based on the XRD results, the diffraction angles were varied from 5 to 90° and measured at a scanning rate of 10°/min. DTA was measured under a nitrogen atmosphere at 50–210 °C. Briefly, five milligrams of the powder was prepared using a simultaneous DTA apparatus DTG-60H (Shimadzu Corp.), and the DTA patterns (melting point) were detected under a nitrogen atmosphere. The temperature was maintained at 5 °C /min.

Dispersibility

Three milliliters of dispersion containing TRO nanoparticles was added to a 5-mL test tube and incubated in the dark at 22 °C for 28 days. Subsequently, images of the dispersions were captured using a digital camera, and 30 μL sample was collected from the upper 90% of the test tube. TRO concentration was determined using HPLC.

Uniformity of the Gels

We divided the TRO gel (0.3 g) into 10 parts (0.03 g) and dissolved it in methanol. Subsequently, the resultant solution was filtered through a 450-nm filter, and the TRO content in the collected samples was measured using HPLC. To evaluate gel uniformity, the standard deviation (S.D.) of TRO content was calculated in 10 gel divisions and expressed as the non-uniformity of TRO in the gel.

Solubility

The gels containing TRO micro- and nanoparticles were diluted 10-fold with purified water at 22 °C, and TRO was separated into soluble and non-solubilized forms by centrifugation at 1×10^5 g using a Beckman OptimaTM MAX-XP Ultracentrifuge (Beckman Coulter, Osaka, Japan). The concentration of soluble TRO was determined using HPLC.

Viscosity

The TRO gel (0.3 g) was set on an SV-1A viscometer (A & D Company, Limited, Tokyo, Japan), and the viscosity was measured at 60 rpm and 22 °C for 3.5 min.

Zeta Potential

The gels containing TRO micro- and nanoparticles were diluted 10-fold with purified water, and then they were set on a model 502 zeta potential analyzer (Nihon Rufuto Co., Ltd., Tokyo, Japan). The zeta potential was analyzed at 49 V and 22 °C for 5 s.

Drug Release from the Gels

A Franz diffusion cell set up with an MF-Millipore™ Membrane Filter 450 μm pore size (Merck Millipore, Tokyo, Japan) was used to determine TRO release from the gels as previously reported.[28–30] Subsequently, 10 mM phosphate buffer (12.2 mL) was added to the reservoir chamber of the cell and 1.5% TRO gel (0.3 g) was placed on the donor side and incubated for 24 h. Thereafter, 50 μL buffer containing TRO was collected from the reservoir chamber at 30 min, 1 h, 2 h, 3 h, 6 h, and 24 h and replaced with the same volume of fresh 10 mM phosphate buffer. The sample concentration was determined using HPLC. Moreover, the 800 μL of samples 24 h after the experiment were injected into NanoSight LM10, and the size and number of TRO nanoparticles in the collected samples were measured after 24 h.

Content of TRO in Gel-Treated Hamsters

We carefully applied 0.1 g of TRO-MP and TRO-NP gels to the hamsters' cheek pouches and kept them there for 3 h and 8 h (n=5×4=20). Subsequently, the hamsters were euthanized under isoflurane anesthesia by injecting pentobarbital (200 mg/kg), and the cheek pouches were carefully removed. In this study, the isoflurane dose was controlled using the Anesthesia Device BS-400TI (Brain Science Idea. Co. Ltd., Osaka, Japan), and the doses used for the induction and maintenance of anesthesia were 4% and 3%, respectively. Blood samples were collected simultaneously. The collected cheek pouches were homogenized in methanol, and both the homogenate and blood were centrifuged at 20.4×10^3 g and 4 °C for 20 min. The supernatants were used as samples, and the TRO content in both the cheek pouches and blood samples was measured using HPLC. Endocytosis was inhibited as previously described.[29] The hamsters were divided into five groups (n=5×5=25) and their cheek pouches were treated with TRO gels containing endocytosis inhibitors for 8 h. Cytochalasin D (phagocytosis inhibitor),[32] 2 μM rottlerin (micropinocytosis inhibitor),[33] 40 μM dynasore [clathrin-dependent endocytosis (CME) inhibitor],[34] and 54 μM nystatin [caveolae-dependent endocytosis (CavME) inhibitor][32] were dissolved in 0.1% dimethyl sulfoxide (DMSO) and mixed with TRO gels, for later use.

Wound Area in the Hamster Model of OM

The golden hamsters were divided into four groups: a non-treated group (n=8), vehicle-treated, TRO-MP gel-treated, and TRO-NP gel-treated groups (n=5×3=15). Each hamster received an injection of 25 μL of 10% acetic acid into the cheek pouches under isoflurane anesthesia. In this study, the isoflurane dose was controlled using the Anesthesia Device BS-400TI, and the doses for induction and maintenance of anesthesia were 4% and 3%, respectively. The hamsters were housed for two days and then they were subsequently used in the experiments. For three days (at 10:00 AM), 0.1 g vehicle and TRO gels were administered to the cheek pouches once daily. The wound area appeared to be more swollen or looked more concave in appearance than under normal conditions. To analyze the wound area, a specific area was selected from each image. While quantifying the wound area, it was difficult to accurately determine the point at which the wound healed completely. Therefore, we have shown results for up to 3 days later when the wound could be determined with certainty. The wound changes were monitored at 9:00 AM on days 0, 1, 2, and 3 using a digital camera. The value (%) of the wound area was calculated as the ratio of the initial wound area. The initial wound areas (at 0 days) for non-treated, vehicle-treated, TRO-MP gel-treated, and TRO-NP gel-treated hamsters were 10.2±0.71, 10.3±3.0, 10.9 ±2.9, and 10.1±2.1 mm^2, respectively [values are represented as mean ± standard error of mean (SEM)].

Statistical Analysis

Data are presented as the mean SEM. Statistical differences were analyzed using the JMP software ver. 5.1 (SAS Institute). One-way repeated-measures analysis of variance (ANOVA) followed by the Tukey–Kramer test was used for the statistical analysis of multiple group comparisons. Statistical differences between the two groups were analyzed using the unpaired Student's *t*-test. A P-value < 0.05 was considered statistically significant.

Results

Characteristics of Gel Formulations Containing TRO Nanoparticles

First, we prepared TRO nanoparticles by bead milling. Particle distributions are illustrated in Figure 1A and B. Bead milling decreased the particle size of TRO from 16.6 μm to 116.8 nm. Moreover, milled TRO exhibited improved dispersibility compared to TRO-sus, and no precipitation occurred within one month of preparation (Figure 1C and D). Furthermore, we evaluated whether bead milling affected the crystal form of TRO (Figure 2). The melting point of TRO was similar between TRO powder (181.05 °C) and TRO-sus (181.12 °C). However, the melting point of TRO in milled TRO decreased to 138.68 °C. Additionally, the XRD pattern of milled TRO was different from that of TRO-sus. Bead milling reduced the number of XRD peaks, resulting in a pattern resembling that of amorphous TRO. Subsequently, gel formulations containing TRO nanoparticles were prepared using the milled TRO (Figure 3). The TRO-NP gel exhibited a more uniform drug content compared to the TRO-NP gel (Figure 4A). Despite the similar solubility and zeta potential of both gels after bead milling (Figure 4B and D), the viscosity of the TRO-NP gel was higher than that of the TRO-MP

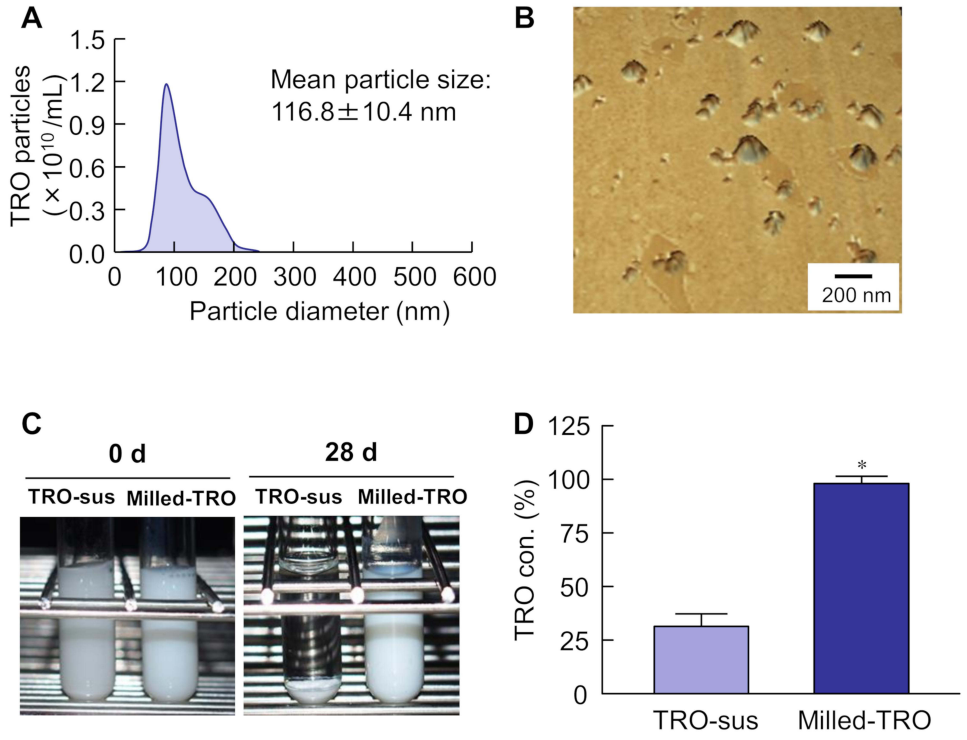

Figure 1 Characteristics of nano-dispersions containing TRO. (**A**) Particle distribution and (**B**) SPM image of dispersions containing milled-TRO. (**C**) Photographs and (**D**) stability of dispersions containing TRO exposed (milled-TRO) or not exposed (TRO-sus) to bead milling. n=8. *P<0.05 vs TRO-sus for each category (Student's t-test). The particle size of milled-TRO was in the range of 50–220 nm, and the stability of dispersions was enhanced by bead milling.

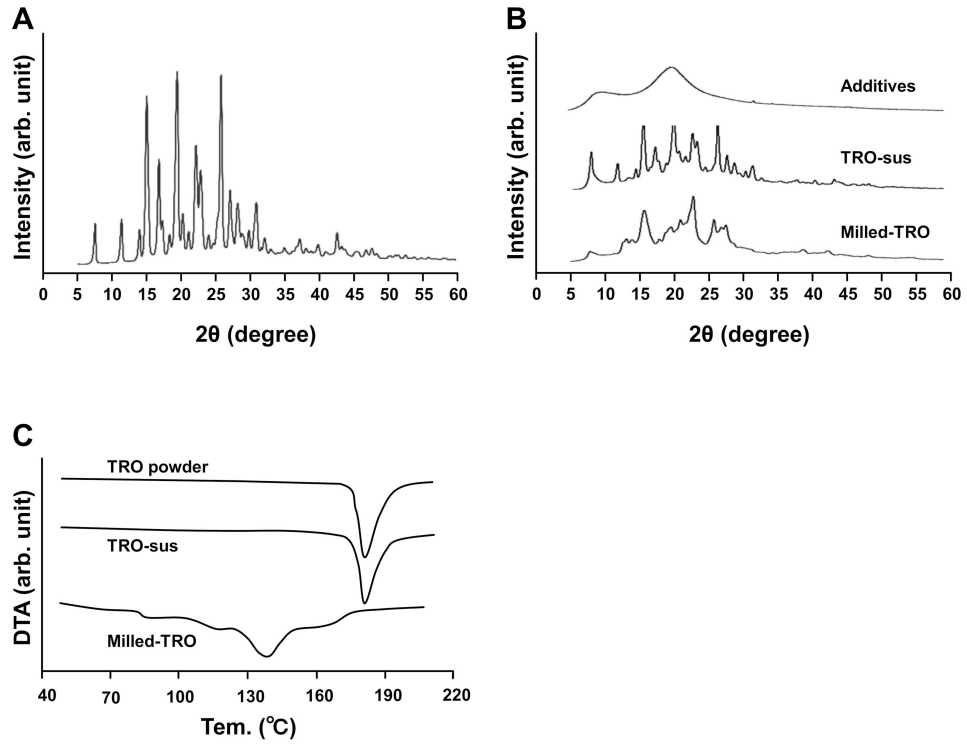

Figure 2 Changes in the XRD pattern and DTA of TRO exposed (milled-TRO) or not exposed (TRO-sus) to bead milling. (**A**) XRD pattern of TRO powder. (**B**) XRD pattern of additives; dispersions contained TRO exposed (milled-TRO) or not exposed (TRO-sus) to bead milling. (**C**) DTA pattern of TRO powder; dispersions contained TRO exposed (milled-TRO) or not exposed (TRO-sus) to bead milling. XRD and DTA patterns of TRO were altered by the bead milling.

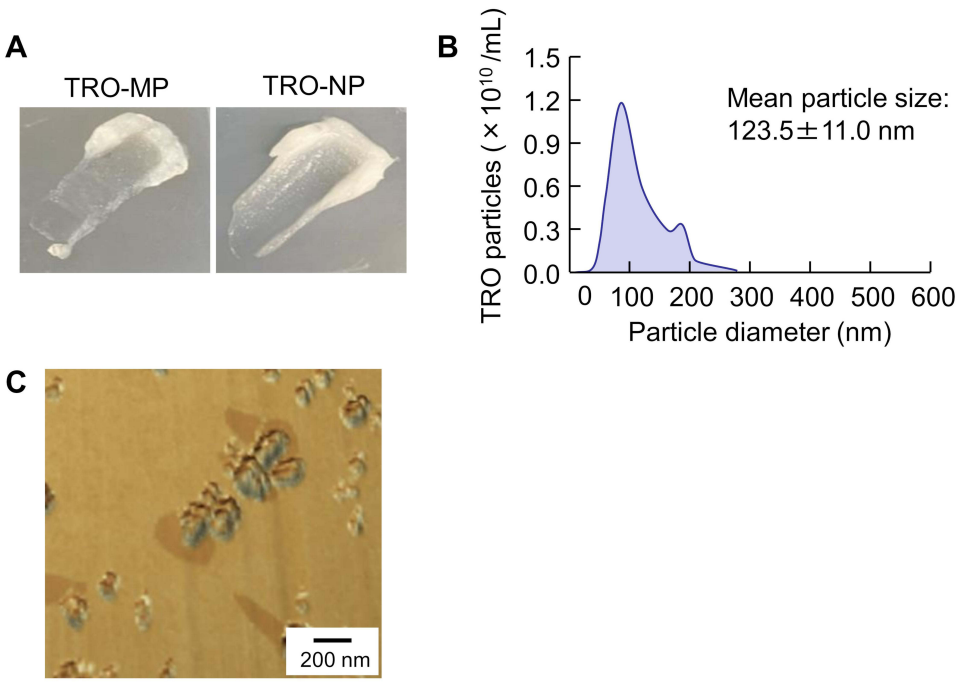

Figure 3 Condition of TRO in gels. (**A**) Photographs of TRO-MP and TRO-NP gels. (**B**) Particle size distribution and (**C**) SPM images of TRO-MP and TRO-NP gels. The particle size of TRO in the TRO-NP gel is in the range of 50–280 nm.

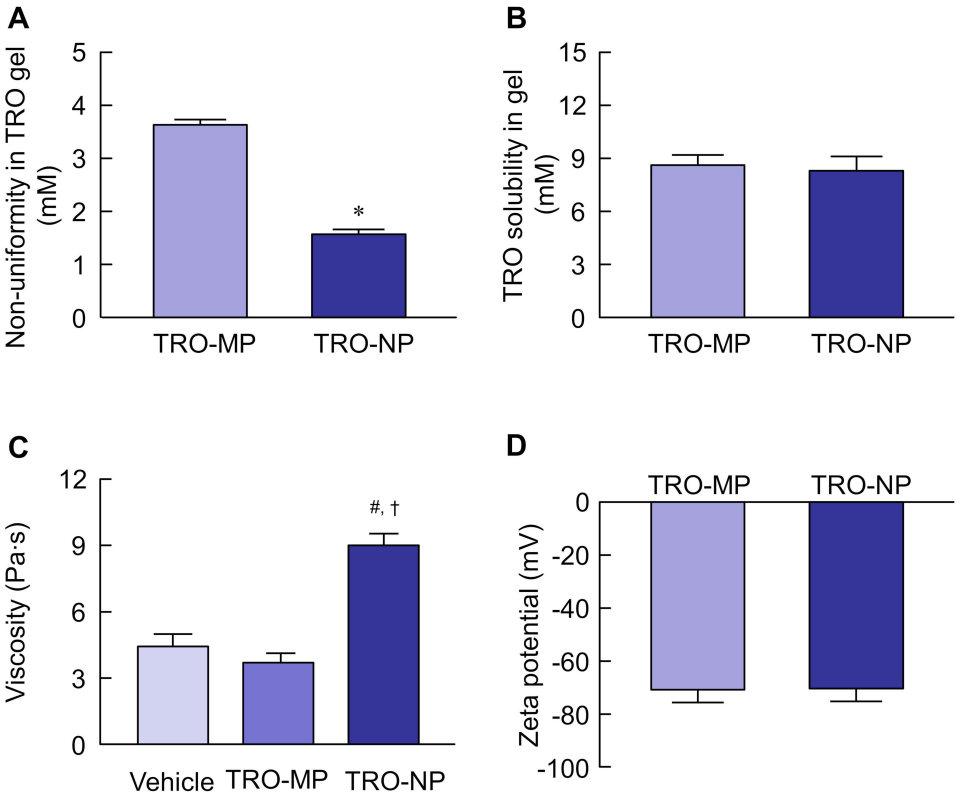

Figure 4 Characteristics of TRO-MP and TRO-NP gels. (**A**) Non-uniformity in TRO particles of TRO-MP and TRO-NP gels. (**B**) Drug solubility, (**C**) viscosity, and (**D**) zeta potential of TRO-MP and TRO-NP gels. n=10. *P<0.05 vs TRO-MP gel for each category (Student's t-test). #P<0.05 vs vehicle for each category (Tukey–Kramer test). #P<0.05 vs TRO-MP gel for each category. †P<0.05 vs TRO-MP gel for each category (Tukey–Kramer test). The uniformity of TRO particles and viscosity of the TRO-NP gel were higher than those of the TRO-MP gel. Conversely, the solubility and zeta potential of TRO was similar in TRO-MP and TRO-NP gels.

gel (Figure 4C). In this study, we measured the viscosity using a tuning fork vibro-viscometer (SV-1A). The principle of these measurements is to resonate an oscillator in the sample, and then we will be able to determine the viscosity from the excitation force required to move the oscillator at a certain amplitude, which shows a correlation with the viscosity.[35] Nanoparticles are widely dispersed, and the required excitation force is considered to be higher than that of microparticles.[35] As a result, the viscosity of the TRO-NP gel may be higher than that of other gels.

Mechanism of TRO Absorption in Cheek Pouch Tissue Treated with TRO-NP Gel

Figure 5 illustrates the release profiles of TRO from TRO-MP and TRO-NP gels. The release of TRO from the TRO-NP gel was higher and included solid TRO nanoparticles and a TRO solution (dissolved TRO). We examined TRO levels in the blood and cheek pouch tissues of hamsters treated with TRO-MP and TRO-NP gels at 3 h and 8 h after treatment. TRO levels in the blood of hamsters treated with TRO-MP and TRO-NP gels were undetectable using HPLC (n=5). Conversely, TRO was detected in the cheek pouch, and 8 h after the treatment, TRO levels in the cheek pouches of hamsters treated with TRO-NP gel were 32.7-fold higher than those treated with TRO-MP gel (Figure 6A). Figure 6B illustrates the relationship between endocytosis and enhanced TRO absorption in the cheek pouch tissue of hamsters treated with TRO-NP gel. TRO levels in TRO-treated hamsters co-treated with nystatin, rotterin, or cytochalasin D were similar to those in the control group (TRO-treated hamsters). In contrast, TRO levels in TRO-treated hamsters co-treated with dynasore were significantly reduced, with the dynasore group exhibiting TRO levels at 66.3% of the control group.

Therapeutic Effect of TRO-NP Gel on OM in the Hamster Model

Figure 7 illustrates the therapeutic potential of TRO-MP and TRO-NP gels for oral wounds. The wound areas in the hamsters injected with acetic acid after 1, 2, and 3 days were 9.10, 8.74, and 8.11 mm^2, respectively (non-treated group). The changes in these wound areas were similar to those observed in the vehicle and TRO-MP groups on days 0–3. In contrast, the TRO-NP gel-treated hamsters evidenced significantly enhanced wound healing, with the wound area in the

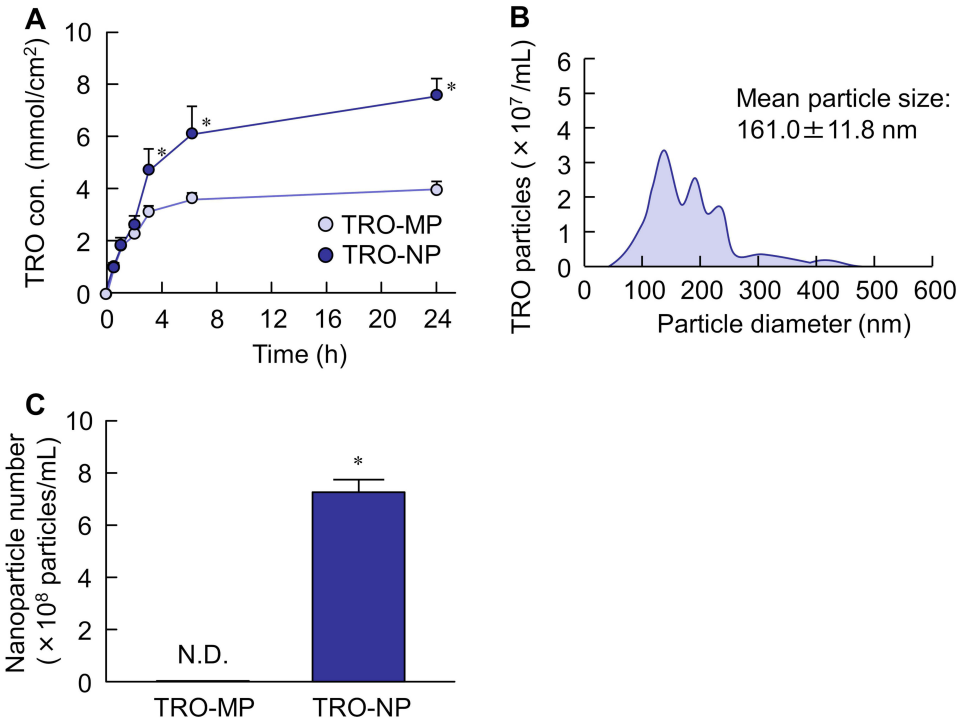

Figure 5 Drug release from TRO-MP and TRO-NP gels through a 220 nm pore membrane. (**A**) Release behavior of TRO from TRO-MP and TRO-NP gels. (**B**) Size distribution and (**C**) number of TRO nanoparticles in the reservoir chamber 24 h after the application of TRO-NP gels. n=6. N.D., not detectable. *P<0.05 vs TRO-MP gel for each category (Student's t-test). The release of TRO from the TRO-NP gel was higher than that from the TRO-MP gel; TRO nanoparticles were detected in the reservoir chamber 24 h after the application of TRO-NP gel.

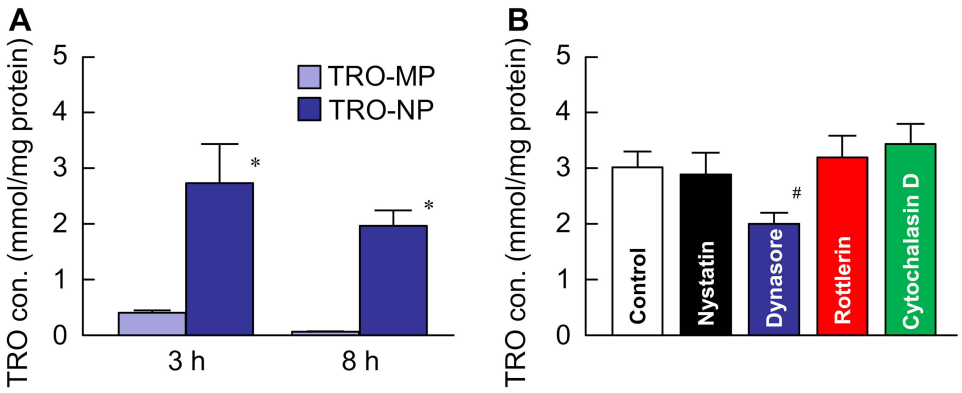

Figure 6 Effect of endocytosis on the content of TRO in cheek pouches of hamsters with OM after treatment with TRO gels. (**A**) Changes in TRO content in the cheek pouches of hamsters 3 h and 8 h after treatment with TRO gels (TRO-MP at 3 h and 8 h, n=5×2=10; TRO-NP at 3 h and 8 h, n=5×2=10). (**B**) Changes in TRO content in the cheek pouches of hamsters 3 h after co-treatment with endocytosis inhibitors and TRO-NP gel. Control, TRO-NP gel-treated hamsters (n=5). Each endocytosis inhibitor-treated hamster [nystatin (n=5), dynasore (n=5), rottlerin (n=5), cytochalasin D (n=5)] was co-treated with TRO-NP gel. Total n=45. *P<0.05 vs TRO-MP gel for each category (Student's t-test). #P<0.05 vs control for each category (Tukey–Kramer test). TRO nanoparticles were taken up via the CME pathway, and TRO levels in the cheek pouches of hamsters treated with the TRO-NP gel were higher than those treated with the TRO-MP gel.

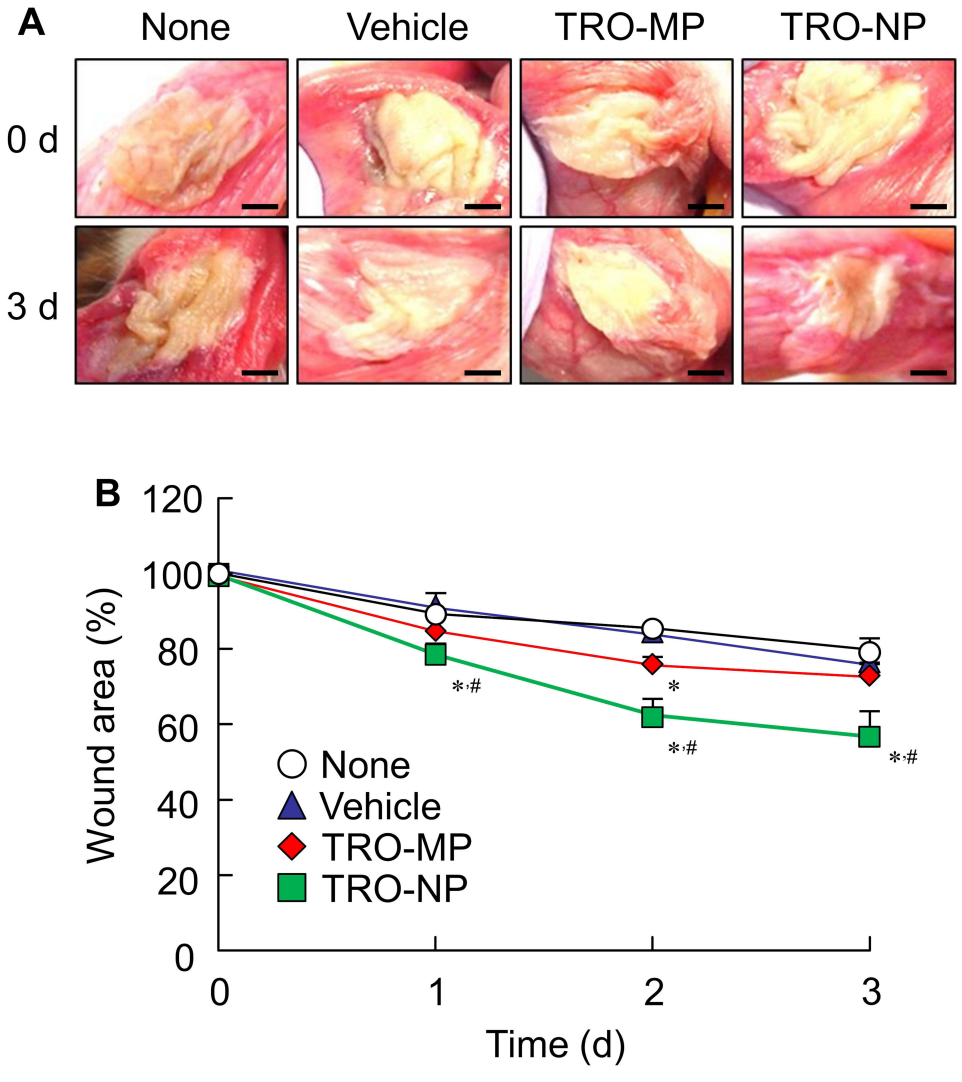

Figure 7 Changes in the wound area in the cheek pouches of hamsters with OM 0–3 days after treatment with TRO gels. (**A**) Representative images and (**B**) wound area of cheek pouches treated with TRO gels. Bar in the image (**A**) indicate 1 mm. Total n=23 [none, n=8; vehicle (n=5), TRO-MP (n=5), and TRO-NP gels (n=5)]. *P<0.05 vs vehicle for each category (Tukey–Kramer test). #P<0.05 vs TRO-MP gel for each category (Tukey–Kramer test). The therapeutic effect of the TRO-NP gel was higher than that of the TRO-MP gel in the cheek pouches of hamsters with OM.

TRO-NP gel-treated groups 3 days after treatment reaching 69% of that in the non-treated group. Moreover, the TRO-NP gel showed the fastest complete healing of the wound when observed visually compared to the other groups.

Discussion

Although medical therapeutic modalities for OM, such as anti-inflammatory agents are widely used,[1,2] these often lack sufficient efficacy in severe cases of OM. To improve treatment outcomes, here we developed a Carbopol gel containing TRO nanoparticles, which demonstrated high wound healing and preventive effects in a hamster model of acetic acid-induced OM.

Build-up and breakdown methods are known to produce solid nanoparticles. Earlier, we utilized a breakdown method based on bead milling using a cellulose compound to obtain solid nanoparticles of indomethacin and tranilast <100 nm.[36,37] Here, we successfully prepared TRO nanoparticles (mean particle size: 116.8 nm; Figure 1) using the bead milling method and found them suitable for producing solid nanoparticles. Next, the crystal forms were investigated using DTA and XRD. In the package insert of APLACE® Fine Granules 20%,[38] it was noted that the melting point of TRO is 177–181 °C. The melting point of TRO measured in this study was similar to the data in the package insert (Figure 2C). On the other hand, we confirmed changes in the crystallized TRO due to bead milling, with the melting point of TRO in the milled TRO being 138.68 °C (Figure 2C). The XRD pattern of TRO slightly resembled that of amorphous TRO (Figure 2A and B), which suggested the presence of a mixture of crystalline and amorphous TRO in the nanoparticles. The solubility might have been higher, if more amorphous TRO were present; however, the solubilities of TRO-NP and TRO-MP were similar, suggesting a mixture. Several peaks were detected in the XRD pattern (Figure 2B), and the solubility of TRO was very low (Figure 4B). Taken together, these results suggest that the amorphous fraction of TRO may not be significant enough in order to alter its solubility. Selection of an appropriate base is important for producing gels containing TRO nanoparticles. Gels are particularly suitable for water-soluble medicaments because they are semi-solid preparations containing large proportions of water and are less suitable for insoluble substances that cannot be easily and uniformly incorporated. However, Carbopol gel is suitable for facilitating drug release from nanoparticle-containing formulations,[28–30] and gels prepared using nanosuspensions can overcome the issue of insoluble substances that cannot be easily and uniformly incorporated into the water-soluble gels.[30] Therefore, for gel formulation in this study, we selected a Carbopol gel as the base to prepare a gel containing TRO nanoparticles. The TRO-NP gel exhibited a higher uniformity of TRO than the TRO-MP gel (Figure 4A),[30] and maintained the TRO nanoparticles within the gel (Figure 3). Here, we have compared the solubility of the prepared TRO gels with related ones in the package insert of troxipide.[38] The solubility of the TRO powder (pKa=10.08) is 5.29 mM in water at 20±5 °C. Carbopol® 934 may increase the solubility of TRO, since the solubility of TRO in the TRO gel (pH 7.5) was approximately 8.6 mM at 22 °C (Figure 4B). The prepared TRO-NP gel was used for subsequent experiments not published yet.

We investigated the release profile of TRO from the TRO-NP gel (Figure 5) and observed higher release compared to the TRO-MP gel, possibly due to the release of nanoparticles facilitated (Figure 5C). On the other hand, the particle size distribution of the released TRO-NP gel particles was larger than that within the gel (Figure 3B). To evaluate TRO release, we used a Franz diffusion cell filled with 10 mM phosphate buffer. The TRO nanoparticles in phosphate buffer were not more stable than those in the gels due to the low viscosity of the buffer, which may have affected nanoparticle aggregation. Furthermore, we measured the changes in TRO levels in the blood and cheek pouches of hamsters treated with TRO-NP gel (Figure 6A). The hamster, owing to its vascularized cheek pouch, is considered an excellent model for reproducing lesion severity in the oral mucosa, similar to that in humans with oral mucositis. Hamsters have been the most used animal models to study the healing, development, and pathways of oral mucositis.[39,40] Therefore, hamsters were used in the in vivo study. TRO permeated the cheek pouches of hamsters treated with TRO-NP gel, resulting in enhanced persistence and accumulation of TRO compared to the TRO-MP gel treatment. These results align with the in vitro study on TRO release from the gels (Figure 5). Previous studies have indicated that particles >1 μm do not accumulate on cell membrane surfaces,[26] while those >500 nm have limited ability to diffuse through the mucin layer.[25] In contrast, particles <500 nm diameter have better mucoadhesive properties and accumulate on the apical membranes of surface epithelial cells.[26] Our present study supports these previous findings.

Nanoparticle uptake pathways can be categorized into receptor-mediated endocytosis (CavME and CME), MP/phagocytosis, and passive penetration. Thus, drug nanoparticles cannot easily enter cells through diffusion.[41,42] Receptor-mediated endocytosis (CavME and CME) can take up nanoparticles with diameter <120 and <80 nm, respectively,[43] while micropinocytosis and phagocytosis take up particles sized between 100 nm–5 μm and 0.5–5 μm, respectively.[41–43] Therefore, we investigated whether penetration of TRO nanoparticles from gels decreased after treatment with inhibitors of energy-dependent endocytosis (nystatin, an inhibitor of CavME;[33] dynasore, an inhibitor of CME;[33] rottlerin, an inhibitor of MP;[34] and cytochalasin D, an inhibitor of phagocytosis)[32] (Figure 6B). Co-treatment with the CME inhibitor attenuated TRO penetration. Although the precise mechanism of nanoparticle penetration remains partially understood, several reports, including our study using rebamipide,[44] demonstrate that chemicals facilitating penetration and reduction in drug size can enhance the cellular uptake of nanoparticles,[45] and that CME influences the uptake and transport of TRO nanoparticles through the cheek pouch tissue. In the mouse model of OM (Figure 6), TRO-MP gel slightly slowed wound repair, as the wound area was significantly smaller on day 2 of treatment than in the control group. In contrast, treatment with TRO-NP gel accelerated the wound healing rate, and the wound area was significantly decreased compared to that in the vehicle-treated and TRO-MP-treated groups 1–3 days after treatment with TRO-NP gel. We hypothesize that TRO promotes wound healing in the oral mucosa of hamsters, and the gel formulation incorporating TRO nanoparticles enhances its therapeutic effect. TRO-NP gel can be a useful therapy for OM. However, in comparison to our previous results on the use of a gel containing rebamipide nanoparticles for an acetic acid-injected OM model,[44] the wound areas in the oral mucosa of the TRO-NP gel-treated group were larger, indicating a weaker therapeutic effect of TRO. Further studies are required to evaluate the wound healing rate in an OM model co-treated with gels containing rebamipide and TRO nanoparticles. Moreover, the mechanism of wound repair using TRO nanoparticles remains to be elucidated. Therefore, we have planned to perform histological examinations using hematoxylin and eosin (H&E) staining and multi-cytokeratin immunostaining.

Conclusion

We formulated a Carbopol gel containing TRO nanoparticles (TRO-NP gel) and demonstrated that CME is involved in the penetration of TRO released from the gel into the cheek pouches of the treated golden hamsters. Additionally, TRO-NP gel treatment enhanced wound healing in the acetic acid-injected OM model. Our study provides evidence that the TRO nanoparticles from the TRO-NP gel are absorbed by the cheek pouch tissue through the CME pathway, resulting in increased wound healing. No hydrogel formulations incorporating TRO nanoparticle have yet been developed. This is the first study that has revealed that certain formulations (TRO-NP gels) are useful for the treatment of stomatitis. In addition, we have found that CME was related to the uptake and transport of TRO nanoparticles through cheek pouch tissue, as the TRO content in the cheek pouch was attenuated by the inhibitor. Thus, these findings are highly novel, and this study for "design of a nanomedicine" will provide a remarkable contribution to the community.

Abbreviations

AFM, atomic force microscopy; CavME, caveolae-dependent endocytosis; CME, clathrin-dependent endocytosis; DTA, differential thermal analysis; MC, methylcellulose; milled-TRO, TRO treated with bead mill; MP, micropinocytosis; OM, oral mucositis; TRO-MP gel, gel formulations based on TRO microparticles; TRO-NP gel, gel formulations based on TRO solid nanoparticles; TRO-sus, TRO suspension; S.E.M., standard error of the mean; S.D., standard deviation; XRD, powder X-ray diffraction.

Data Sharing Statement

The data generated in the present study may be requested from the corresponding author.

Ethics Approval

All animal experiments were performed in accordance with the guidelines of the Kindai University, Japanese Pharmacological Society, and NIH. The experimental protocols were approved on April 1, 2019, by Kindai University

under the project identification code KAPS-31-016, and the study was carried out in compliance with the ARRIVE guidelines and the AVMA euthanasia guidelines 2020.

Author Contributions

All authors made a significant contribution to the work reported, whether that was in the conception, study design, execution, acquisition of data, analysis, and interpretation, or in all of these areas. All authors took part in either drafting, revising, or critically reviewing the article, and they all gave final approval of the version to be published. All authors agreed on the journal to which the article has been submitted, and they agreed to be accountable for all aspects of the work.

Funding

We gratefully acknowledge the funding received from the Ministry of Education, Culture, Sports, Science, and Technology of Japan (Grant No. 21K06656).

Disclosure

The authors report no conflicts of interest in this work.

References

1. Bolouri AJ, Pakfetrat A, Tonkaboni A, et al. Preventing and therapeutic effect of propolis in radiotherapy induced mucositis of head and neck cancers: a triple-blind, randomized, placebo-controlled trial. *Iran J Cancer Prev*. 2015;8:e4019.
2. Lalla RV, Sonis ST, Peterson DE. Management of oral mucositis in patients who have cancer. *Dent Clin North Am*. 2008;52(1):61–77. doi:10.1016/j.cden.2007.10.002
3. Bian L, Han G, Zhao CW, Gari PJ, Wang X-J. The role of Smad7 in oral mucositis. *Protein Cell*. 2015;6(3):160–169. doi:10.1007/s13238-014-0130-4
4. Shimamura Y, Takeuchi I, Terada H, Makino K. A mouse model for oral mucositis induced by cancer chemotherapy. *Anticancer Res*. 2018;38(1):307–312. doi:10.21873/anticanres.12223
5. Kusugami K, Ina K, Hosokawa T, et al. Troxipide, a novel antiulcer compound, has inhibitory effects on human neutrophil migration and activation induced by various stimulants. *Dig Liver Dis*. 2000;32(4):305–311. doi:10.1016/S1590-8658(00)80023-7
6. Momo K, Hoshina K, Ishibashi Y, Saito T. [Preventive effects of troxipide on a newly developed model of acute gastric mucosal lesion (AGML) induced by ischemia/reperfusion plus ammonia in the rat]. *Nihon Yakurigaku Zasshi*. 1994;104(4):313–323. Japanese. doi:10.1254/fpj.104.313
7. Inoue M, Takahashi M, Ishibashi Y, Sueyoshi S, Kobayashi F, Matsuzawa S. Effects of troxipide on the prednisolone-induced aggravation of gastric mucosal lesions occurred by HC1 in rats. *Jpn Pharmacol Ther*. 2005;33:757–763.
8. Wang J, Zhang L, Fang Z, Fan A, Wang Y. [The pharmacodynamics of troxipide on experimental gastric ulcers in rats]. *J West China Univ Med Sci*. 1993;24:313–316. Chinese.
9. Matsui H, Murata Y, Kobayashi F, et al. Diclofenac-induced gastric mucosal fluorescence in rats. *Dig Dis Sci*. 2001;46(2):338–344. doi:10.1023/A:1005656916830
10. Mine T, Kataoka A, Fujisaki J, et al. Effects of cimetidine and troxipide on gastric mucosal prostaglandin synthesis in patients with chronic gastric ulcer. *Curr Ther Res*. 1991;50:878–887.
11. Jagdale SC, Kamble SB, Kuchekar BS, Chabukswar AR. Design and evaluation of polyox and pluronic controlled gastroretentive delivery of troxipide. *J Drug Deliv*. 2014;2014:804616. doi:10.1155/2014/804616
12. Almeida H, Amaral MH, Lobão P, Sousa Lobo JM. In situ gelling systems: a strategy to improve the bioavailability of ophthalmic pharmaceutical formulations. *Drug Discov Today*. 2014;19(4):400–412. doi:10.1016/j.drudis.2013.10.001
13. Zhu Q, Wei Y, Li C, Mao S. Inner layer-embedded contact lenses for ion triggered controlled drug delivery. *Mater Sci Eng C Mater Biol Appl*. 2018;93:36–48. doi:10.1016/j.msec.2018.07.065
14. Sun D, Maeno H, Gujrati M, et al. Self-assembly of a multifunctional lipid with core-shell dendrimer DNA nanoparticles enhanced efficient gene delivery at low charge ratios into RPE cells. *Macromol Biosci*. 2015;15(12):1663–1672. doi:10.1002/mabi.201500192
15. Grimaudo MA, Pescina S, Padula C, et al. Topical application of polymeric nanomicelles in ophthalmology: a review on research efforts for the non-invasive delivery of ocular therapeutics. *Expert Opin Drug Deliv*. 2019;16(4):397–413. doi:10.1080/17425247.2019.1597848
16. Service RF. Nanotoxicology. Nanotechnology grows up. *Science*. 2004;304(5678):1732–1734. doi:10.1126/science.304.5678.1732
17. Alahmadi M, Alsaedi WH, Mohamed WS, Hassan HMA, Ezzeldien M, Adu-Dief AM. Development of Bi2O3/MoSe2 mixed nanostructures for photocatalytic degradation of methylene blue dye. *J Taibah Univ Sci*. 2023;17(1):2161333. doi:10.1080/16583655.2022.2161333
18. Hosny S, Abd El-Baki RF, Abd El-Wahab ZH, et al. Development of novel nano-sized imine complexes using Coriandrum sativum extract: structural elucidation, non-isothermal kinetic study, theoretical investigation and pharmaceutical applications. *Int J Mol Sci*. 2023;24(18):14259. doi:10.3390/ijms241814259
19. Salaheldeen M, Nafady A, Adu-Dief AM, et al. Enhancement of exchange bias and perpendicular magnetic anisotropy in CoO/Co multilayer thin films by tuning the alumina template nanohole size. *Nanomaterials*. 2022;12(15):2544. doi:10.3390/nano12152544
20. Adu-Dief AM, Essawy AA, Diab AK, Mohamed WS. Facile synthesis and characterization of novel Gd2O3–CdO binary mixed oxide nanocomposites of highly photocatalytic activity for wastewater remediation under solar illumination. *J Phys Chem Solids*. 2021;148:109666. doi:10.1016/j.jpcs.2020.109666

21. Adu-Dief AM, Mohamed WS. Development of nanomaterials as photo catalysts for environmental applications. *Curr Catal*. 2020;9(2):128–137. doi:10.2174/2211544709999201123193710
22. Doak SH, Griffiths SM, Manshian B, et al. Confounding experimental considerations in nanogenotoxicology. *Mutagenesis*. 2009;24(4):285–293. doi:10.1093/mutage/gep010
23. de Jong WH, Borm PJA. Drug delivery and nanoparticles: applications and hazards. *Int J Nanomedicine*. 2008;3:133–149. doi:10.2147/IJN.S596
24. Sanders NN, de Smedt SC, van Rompaey E, Simoens P, de Baets F, Demeester J. Cystic fibrosis sputum: a barrier to the transport of nanospheres. *Am J Respir Crit Care Med*. 2000;162(5):1905–1911. doi:10.1164/ajrccm.162.5.9909009
25. Norris DA, Sinko PJ. Effect of size, surface charge and hydrophobicity on the translocation of polystyrene microspheres through gastrointestinal mucin. *J Appl Polym Sci*. 1997;63(11):1481–1492. doi:10.1002/(SICI)1097-4628(19970314)63:11<1481::AID-APP10>3.0.CO;2-5
26. Szentkuti L. Light microscopical observations on luminally administered dyes, dextrans, nanospheres and microspheres in the pre-epithelial mucus gel layer of the rat distal colon. *J Control Release*. 1997;46(3):233–242. doi:10.1016/S0168-3659(96)01600-8
27. Bravo-Osuna I, Vauthier C, Farabollini A, Palmieri GF, Ponchel G. Mucoadhesion mechanism of chitosan and thiolated chitosan-poly(isobutyl cyanoacrylate) core-shell nanoparticles. *Biomaterials*. 2007;28(13):2233–2243. doi:10.1016/j.biomaterials.2007.01.005
28. Nagai N, Iwamae A, Tanimoto S, Yoshioka C, Ito Y. Pharmacokinetics and antiinflammatory effect of a novel gel system containing ketoprofen solid nanoparticles. *Biol Pharm Bull*. 2015;38(12):1918–1924. doi:10.1248/bpb.b15-00567
29. Nagai N, Ogata F, Otake H, Nakazawa Y, Kawasaki N. Design of a transdermal formulation containing raloxifene nanoparticles for osteoporosis treatment. *Int J Nanomedicine*. 2018;13:5215–5229. doi:10.2147/IJN.S173216
30. Nagai N, Ishii M, Seiriki R, et al. Novel sustained-release drug delivery system for dry eye therapy by rebamipide nanoparticles. *Pharmaceutics*. 2020;12(2):155. doi:10.3390/pharmaceutics12020155
31. American Veterinary Medical Association. *AVMA Guidelines for the Euthanasia of Animals*. American Veterinary Medical Association; 2020.
32. Mäger I, Langel K, Lehto T, Eiríksdóttir E, Langel U. The role of endocytosis on the uptake kinetics of luciferin-conjugated cell-penetrating peptides. *Biochim Biophys Acta*. 2012;1818(3):502–511. doi:10.1016/j.bbamem.2011.11.020
33. Hufnagel H, Hakim P, Lima A, Hollfelder F. Fluid phase endocytosis contributes to transfection of DNA by PEI-25. *Mol Ther*. 2009;17(8):1411–1417. doi:10.1038/mt.2009.121
34. Malomouzh AI, Mukhitov AR, Proskurina SE, Vyskocil F, Nikolsky EE. The effect of dynasore, a blocker of dynamin-dependent endocytosis, on spontaneous quantal and non-quantal release of acetylcholine in murine neuromuscular junctions. *Dokl Biol Sci*. 2014;459(1):330–333. doi:10.1134/S0012496614060052
35. Gotoh K, Yokoshi Y, Nakaso K, Mino Y, Ishizuka H, Nishizuka M. Measurement of apparent powder viscosity by tuning-fork vibration viscometer. *J Soc Powder Technol Japan*. 2021;58(5):250–254. doi:10.4164/sptj.58.250
36. Nagai N, Ito Y, Okamoto N, Shimomura Y. A nanoparticle formulation reduces the corneal toxicity of indomethacin eye drops and enhances its corneal permeability. *Toxicology*. 2014;319:53–62. doi:10.1016/j.tox.2014.02.012
37. Nagai N, Ono H, Hashino M, Ito Y, Okamoto N, Shimomura Y. Improved corneal toxicity and permeability of tranilast by the preparation of ophthalmic formulations containing its nanoparticles. *J Oleo Sci*. 2014;63(2):177–186. doi:10.5650/jos.ess13082
38. APLACE® Fine Granules 20% (troxipide) [package insert]. Tokyo: KYORIN Pharmaceutical Co., 2019.
39. Chor A, Skeff MA, Takiya C, et al. Emerging approaches of wound healing in experimental models of high-grade oral mucositis induced by anticancer therapy. *Oncotarget*. 2021;12(22):2283–2299. doi:10.18632/oncotarget.28091
40. Katayama S, Nishizawa K, Hirano M, Yamamura S, Momose Y. Effect of polaprezinc on healing of acetic acid-induced stomatitis in hamsters. *J Pharm Pharm Sci*. 2000;3(1):114–117.
41. Rappoport JZ. Focusing on clathrin-mediated endocytosis. *Biochem J*. 2008;412(3):415–423. doi:10.1042/BJ20080474
42. Wang J, Byrne JD, Napier ME, DeSimone JM. More effective nanomedicines through particle design. *Small*. 2011;7(14):1919–1931. doi:10.1002/smll.201100442
43. Zhang S, Li J, Lykotrafitis G, Bao G, Suresh S. Size-dependent endocytosis of nanoparticles. *Adv Mater*. 2009;21(4):419–424. doi:10.1002/adma.200801393
44. Nagai N, Seiriki R, Deguchi S, et al. Hydrogel formulations incorporating drug nanocrystals enhance the therapeutic effect of rebamipide in a hamster model for oral mucositis. *Pharmaceutics*. 2020;12(6):532. doi:10.3390/pharmaceutics12060532
45. Shim J, Kang HS, Park W-S, Han S-H, Kim J, Chang I-S. Transdermal delivery of mixnoxidil with block copolymer nanoparticles. *J Control Release*. 2004;97(3):477–484. doi:10.1016/S0168-3659(04)00167-1